Supporting Information

Theoretical investigation into Graphene-Supported Single-Atom Catalysts for Electrochemical CO_2 Reduction

Xiting Wang[a], Huan Niu[a], Yuanshuang Liu[b], Chen Shao,[a] John Robertson,[a] Zhaofu Zhang[c],* and Yuzheng Guo[a],*

[a] School of Electrical Engineering, Wuhan University, Wuhan, Hubei 43072, China

[b] State Key Laboratory of Tribology, School of Mechanical Engineering, Tsinghua University, Beijing, 10084, China

[c] Department of Engineering, Cambridge University, Cambridge, CB2 1PZ, United Kingdom

Corresponding Author

* E-mail: zz389@cam.ac.uk

* E-mail: yguo@whu.edu.cn

Table S1. The difference on E_{bind}-E_{coh} with vdW and without vdW in the substitution models during CO_2 reduction process.

	E_{bind}-E_{coh} with vdW (eV)	**E_{bind}-E_{coh} without vdW (eV)**	**ΔE (eV)**
V@Gr_s	-1.8	-1.93	0.13
Cr@Gr_s	-2.06	-2.07	0.01
Mn@Gr_s	-1.89	-1.79	-0.1
Fe@Gr_s	-2.35	-2.24	-0.11
Co@Gr_s	-2.53	-2.47	-0.06
Ni@Gr_s	-1.88	-1.86	-0.02
Cu@Gr_s	0.02	-0.06	0.08
Zn@Gr_s	-0.14	-0.07	-0.08
Rh@Gr_s	-2.32	-2.46	0.14

Table S2. Calculated Zero-point energies, entropies, and Gibbs free energies of *COOH in the substitution models during CO_2 reduction process.

	E_{ZPE} (eV)	TS (eV)	G (eV)
V@Gr_s	0.62	0.23	-483.91
Cr@Gr_s	0.62	0.26	-484.14
Mn@Gr_s	0.61	0.25	-484.02
Fe@Gr_s	0.60	0.20	-483.12
Co@Gr_s	0.61	0.20	-482.09
Ni@Gr_s	0.61	0.26	-479.67
Cu@Gr_s	0.61	0.13	-476.12
Zn@Gr_s	0.61	0.30	-473.54
Nb@Gr_s	0.63	0.23	-484.62
Mo@Gr_s	0.64	0.20	-484.96
Ru@Gr_s	0.61	0.20	-483.71
Rh@Gr_s	0.60	0.19	-482.21
Pd@Gr_s	0.61	0.26	-478.94
Ag@Gr_s	0.61	0.26	-474.30
W@Gr_s	0.63	0.21	-486.47
Re@Gr_s	0.60	0.14	-485.90
Ir@Gr_s	0.61	0.19	-483.78
Pt@Gr_s	0.61	0.20	-480.35
Au@Gr_s	0.62	0.26	-475.56

* Zero-point energies means that the ground state for the vacuum for electromagnetic fields has a non-zero energy. At the TM@Grs, the values of ZPE is analogical by different inlaid TMs.

Table S3. Calculated Zero-point energies, entropies, and Gibbs free energies of *CO in the substitution models during CO_2 reduction process.

	E_{ZPE} (eV)	TS (eV)	G (eV)
V@Gr_s	0.16	0.20	-472.47
Cr@Gr_s	0.19	0.18	-473.68
Mn@Gr_s	0.19	0.17	-473.50
Fe@Gr_s	0.20	0.16	-472.88
Co@Gr_s	0.20	0.18	-471.61
Ni@Gr_s	0.20	0.16	-469.29
Cu@Gr_s	0.19	0.19	-465.99
Zn@Gr_s	0.19	0.17	-463.16
Nb@Gr_s	0.16	0.21	-473.03
Mo@Gr_s	0.17	0.16	-473.27
Ru@Gr_s	0.20	0.17	-473.64
Rh@Gr_s	0.20	0.10	-471.78
Pd@Gr_s	0.20	0.17	-468.60
Ag@Gr_s	0.18	0.13	-463.92
W@Gr_s	0.16	0.17	-474.78
Re@Gr_s	0.18	0.14	-474.75
Ir@Gr_s	0.21	0.16	-473.28
Pt@Gr_s	0.21	0.15	-470.13
Au@Gr_s	0.20	0.17	-465.10

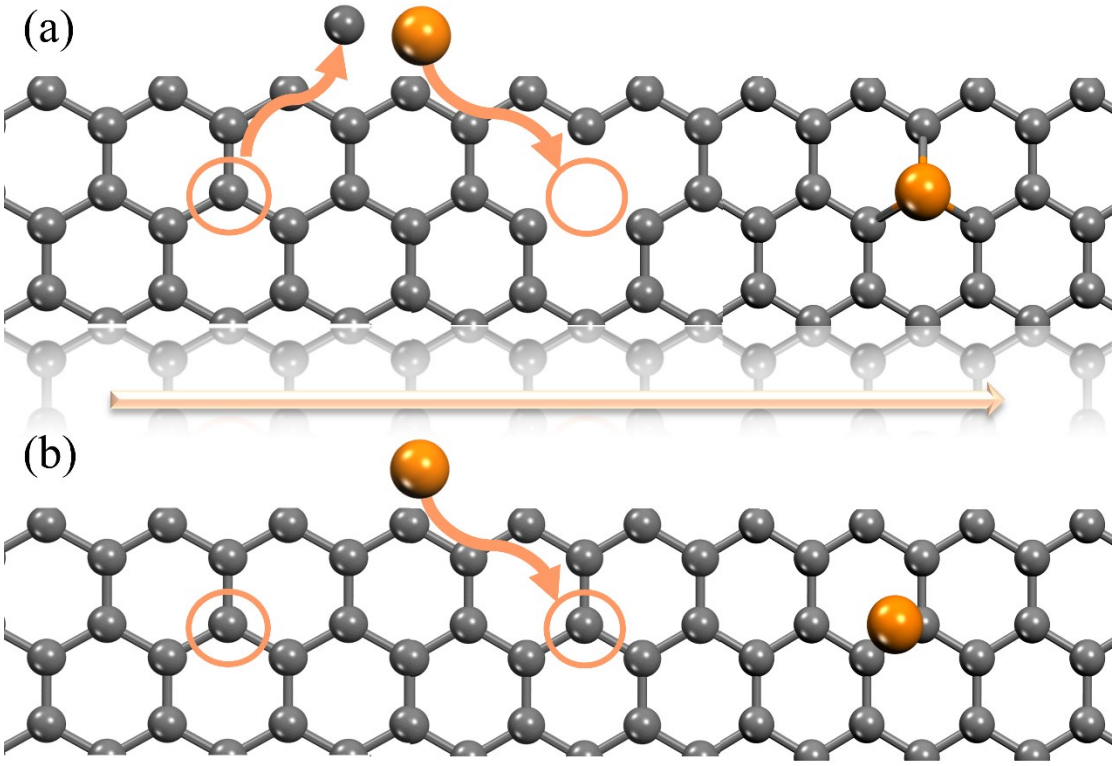

Fig. S1. The schematic illustration of the difference between TM@Gr_s model and TM@Gr_a model. (a) TM@Gr_s is that a transition metal adsorbed on the defected graphene, replacing a carbon atom. (b) TM@Gr_a is that a transition metal adsorbed on the pristine graphene surface, without carbon atom defect.

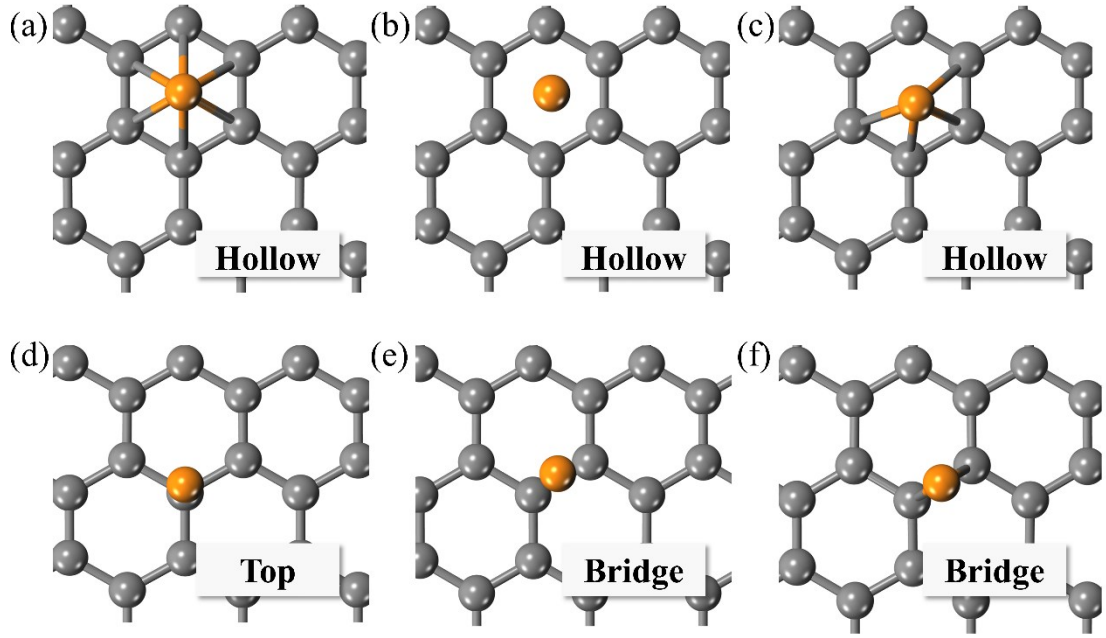

Fig. S2. Top-view of the adsorption models for TM@Gr_a. The hollow type for V@Gr_a, Co@Gr_a, Ni@Gr_a, Nb@Gr_a, Ru@Gr_a, Rh@Gr_a, the top type for Mn@Gr_a, Fe@Gr_a, Cu@Gr_a, Zn@Gr_a, Mo@Gr_a, Ag@Gr_a, Re@Gr_a, Au@Gr_a, the bridge types for Cr@Gr_a, Pd@Gr_a, W@Gr_a, Ir@Gr_a, Pt@Gr_a.

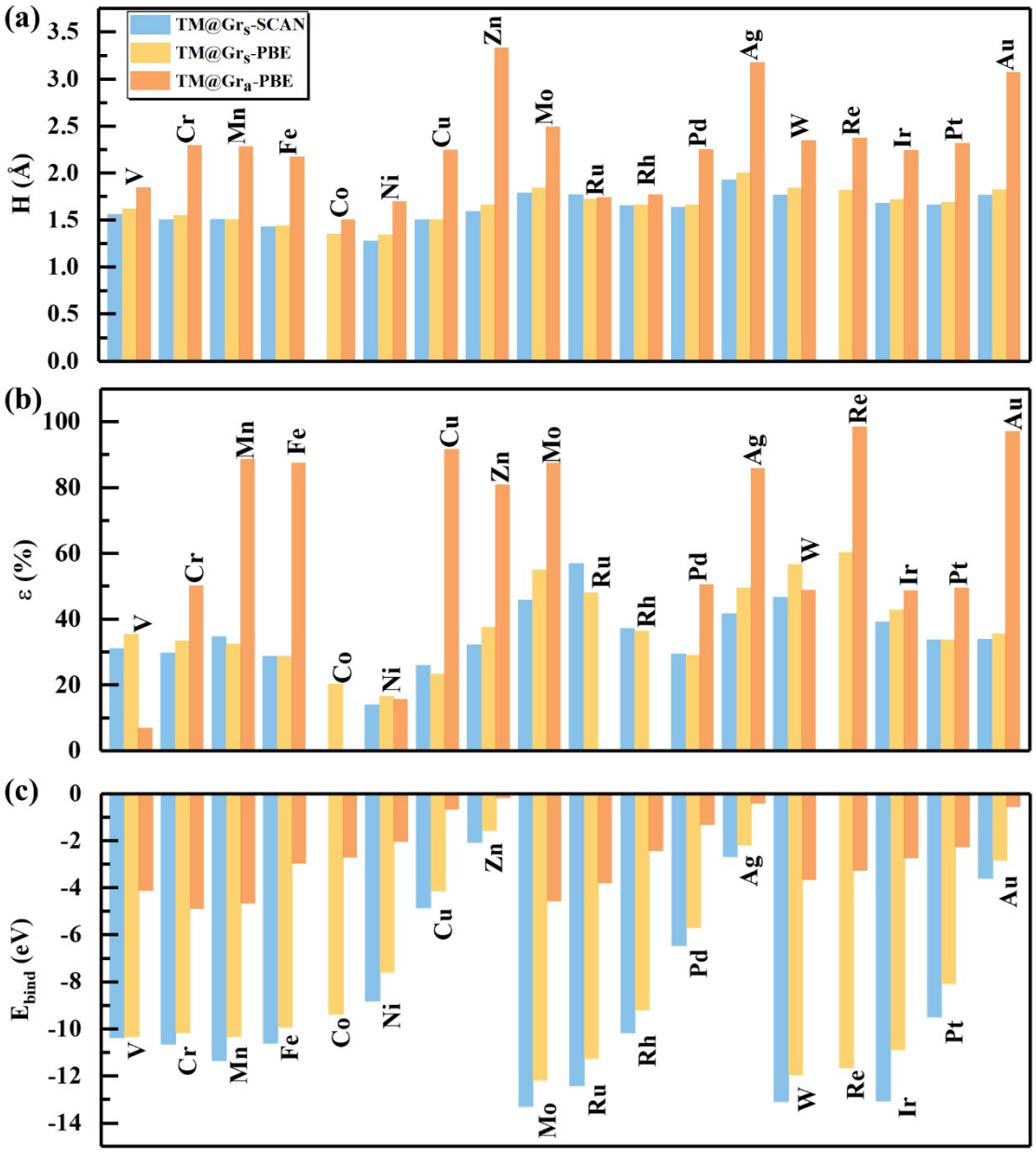

Fig. S3. (a) The elevation (H) from TM to the graphene sheet, (b) the deviation degree (ε) between TM and the graphene plane, and (c) the binding energy (E_{bind}) of TM@Gr$_s$ and TM@Gr$_a$, with SCAN and PBE functionals, respectively.

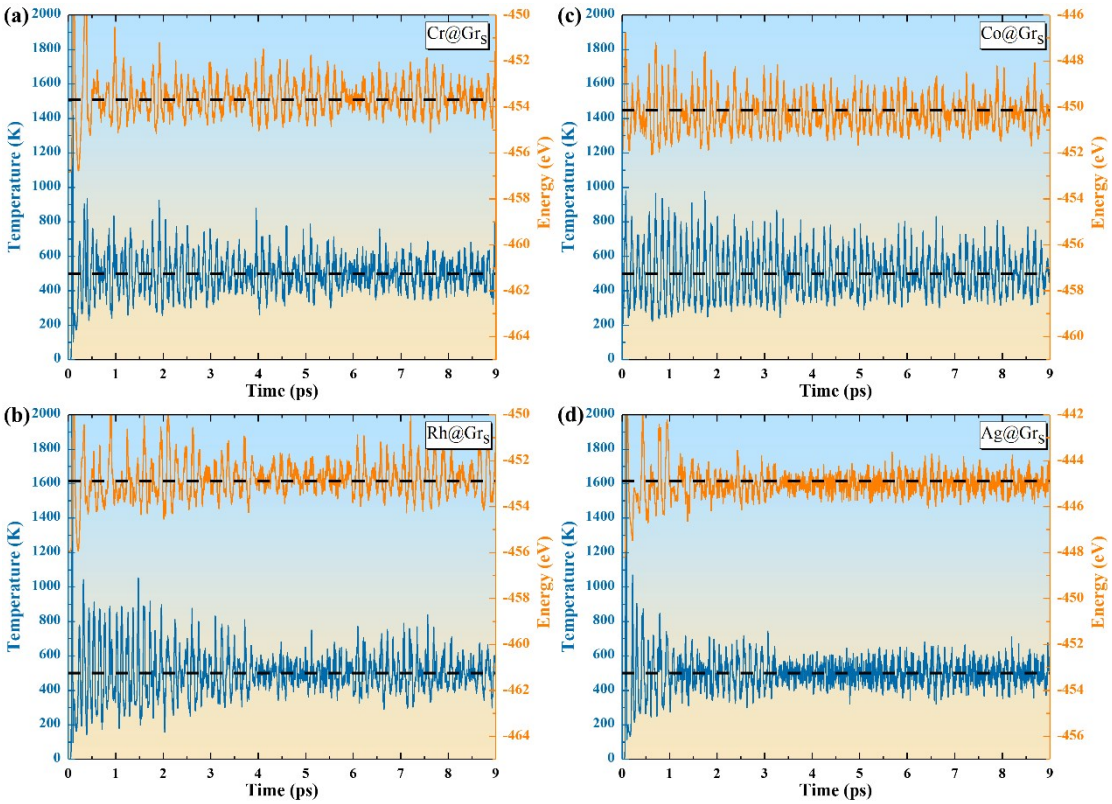

Fig. S4. Variations of energy and temperature versus the AIMD simulation time for $Cr@Gr_s$, $Co@Gr_s$, $Rh@Gr_s$, $Ag@Gr_s$. The simulation lasts for 9 ps at 500 K.

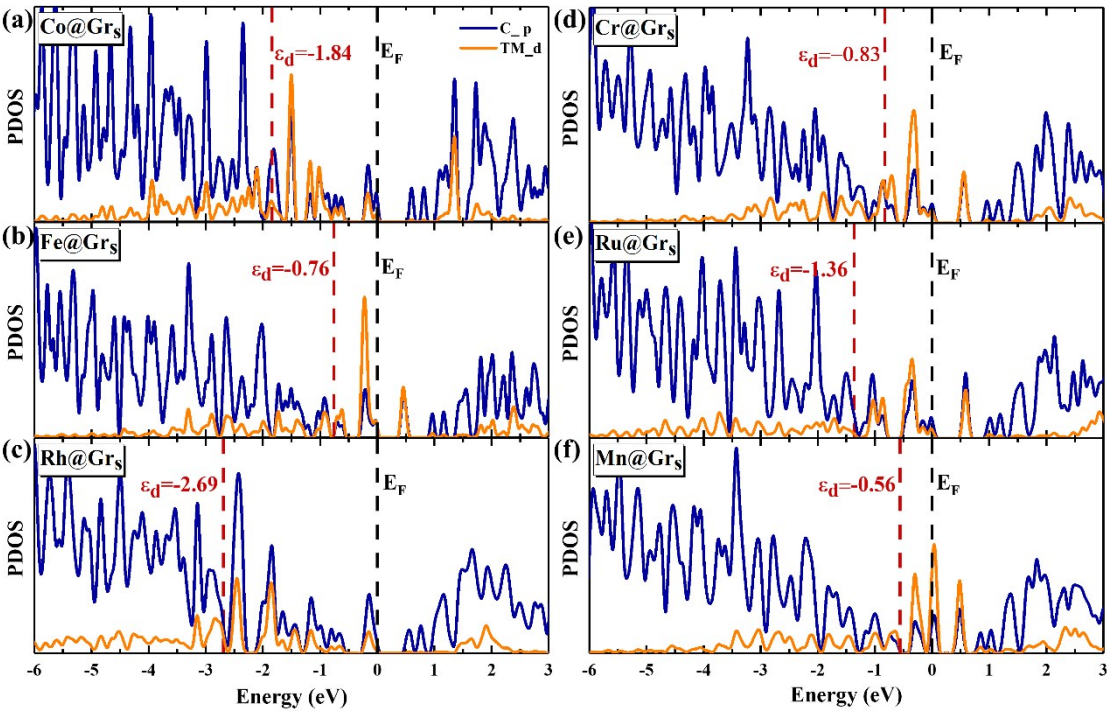

Fig. S5. The projected density of states (PDOS) for (a) $Co@Gr_s$, (b) $Fe@Gr_s$, (c) $Rh@Gr_s$, (d) $Cr@Gr_s$, (e) $Ru@Gr_s$, and (f) $Mn@Gr_s$, respectively. ε_d represents d-band center. E_F denotes the Fermi level and is set to zero. The arrangement order is sorted according to the value of E_{bind}-E_{coh} of Fig. 2d.

As can been seen, the systems exhibit plenty of sharp peaks and have a metallic at the Fermi level. Because of the hybridization between carbon sp^2 and metal d orbitals, especially the orbital overlapping near the Fermi level, there is a strong binding between each other by TM@Gr_s. Besides, there are fewer overlaps between TM d orbitals and graphene near E_F for TM@Gr_s, which TM belongs to the IB group, the tendency is consistent with the weaker interaction.

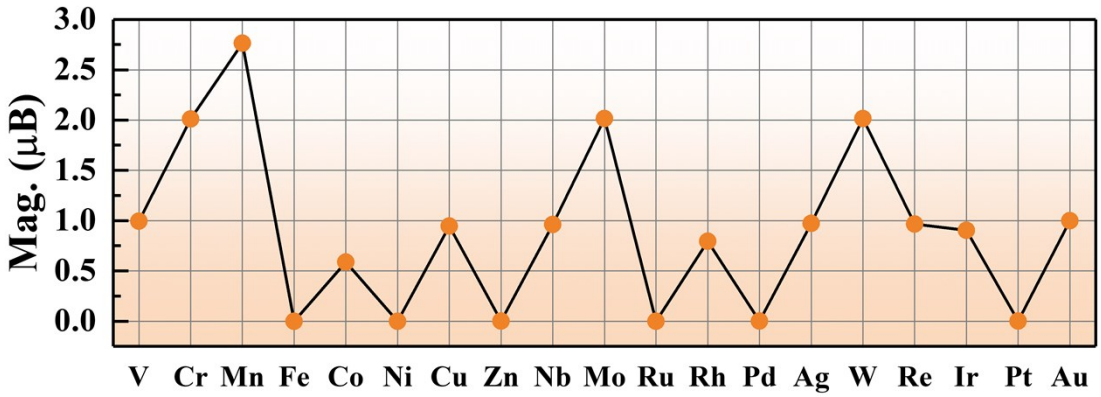

Fig. S6. Total magnetic moments of TM@Gr_s systems.

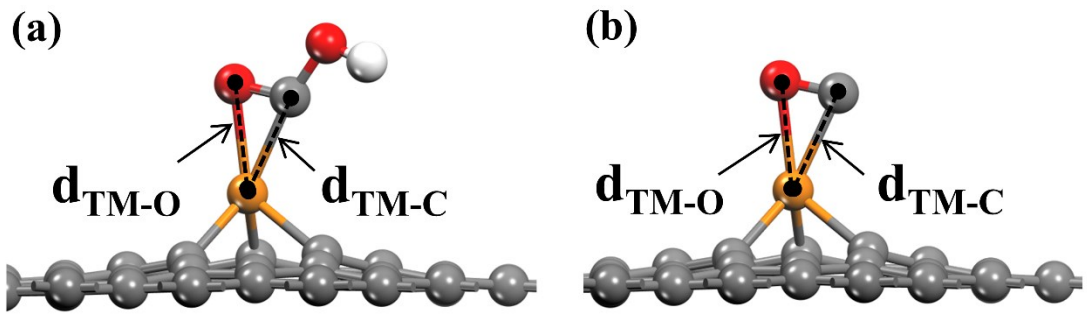

Fig. S7. Atomic structures of (a) TM@Gr_s with adsorbed COOH and (b) TM@Gr_s with adsorbed CO. The bond length in Table S3 and S4 are labelled, respectively.

Table S4. Bond lengths and adsorption energies of COOH in the substitution models.

	d_{TM-C} (Å)	d_{TM-O} (Å)	E_b (eV)
V@Gr_s	2.06	2.08	-2.72
Cr@Gr_s	2.01	2.14	-2.28
Mn@Gr_s	1.98	2.22	-2.94
Fe@Gr_s	1.96	2.72	-2.34
Co@Gr_s	1.95	2.72	-2.32
Ni@Gr_s	1.89	2.28	-2.04
Cu@Gr_s	1.90	2.42	-2.03
Zn@Gr_s	1.99	2.80	-2.08
Nb@Gr_s	2.23	2.18	-3.03
Mo@Gr_s	2.03	2.27	-2.71
Ru@Gr_s	2.09	2.76	-2.08
Rh@Gr_s	2.11	2.79	-2.17
Pd@Gr_s	2.07	2.65	-1.90
Ag@Gr_s	2.10	2.81	-2.10
W@Gr_s	2.13	2.17	-3.01
Re@Gr_s	2.10	2.44	-2.80
Ir@Gr_s	2.09	2.75	-2.73
Pt@Gr_s	2.05	2.59	-2.20
Au@Gr_s	2.07	2.79	-2.80

* The schematic diagram is shown in Fig. S7 (a). The distance between carbon atoms and TM is shorter than the distance of oxygen atoms and TM. And the binding energy is in the range of -3.03 eV to-2.03 eV.

Table S5. Bond lengths and adsorption energies of CO in the substitution models.

	d_{TM-C} (Å)	d_{TM-O} (Å)	E_b (eV)
V@Gr_s	2.14	2.14	-0.60
Cr@Gr_s	1.96	3.12	-1.13
Mn@Gr_s	1.90	3.06	-1.73
Fe@Gr_s	1.87	3.03	-1.42
Co@Gr_s	1.83	2.99	-1.17
Ni@Gr_s	1.85	3.00	-0.99
Cu@Gr_s	1.84	3.00	-1.22
Zn@Gr_s	1.90	3.05	-1.03
Nb@Gr_s	2.39	2.39	-0.66
Mo@Gr_s	2.23	2.23	-0.34
Ru@Gr_s	1.98	3.14	-1.33
Rh@Gr_s	1.98	3.14	-1.06
Pd@Gr_s	2.03	3.18	-0.89
Ag@Gr_s	1.96	3.14	-1.04
W@Gr_s	2.23	2.26	-0.64
Re@Gr_s	2.15	2.23	-0.97
Ir@Gr_s	1.95	3.12	-1.55
Pt@Gr_s	1.96	3.12	-1.30
Au@Gr_s	1.94	3.10	-1.67

* The schematic diagram is shown in Fig. S7 (b). The position of C atoms is closer to TMs than the corresponding O atoms. The adsorption energy of COOH is lower than that of CO on TM@Gr_s.

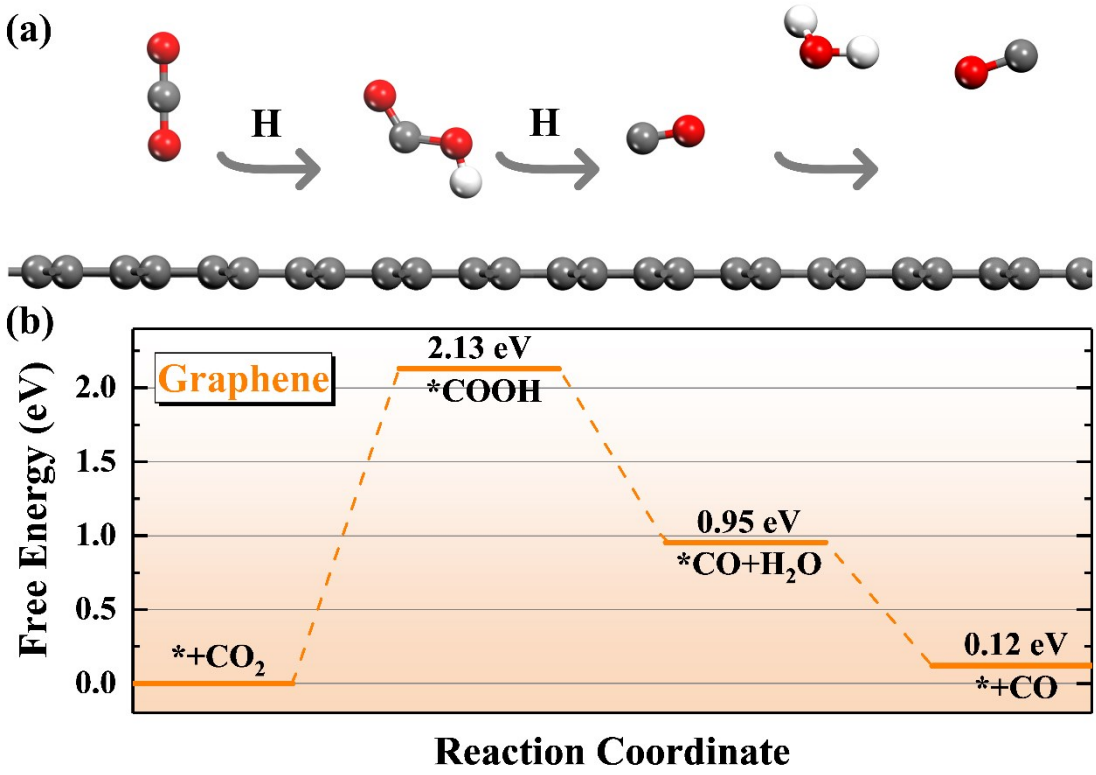

Fig. S8. The Gibbs free energy diagram of CO_2 hydrogenation to CO on the pristine graphene sheet.

	VB	VIB	VIIB	VIII			IB	IIB
3d	V -0.72	Cr -0.21	Mn -0.81	Fe -0.49	Co -0.24	Ni -0.40	Cu -0.42	Zn -0.36
4d	Nb -0.88	Mo -0.97		Ru -0.41	Rh -0.27	Pd -0.54	Ag -0.34	
5d		W -0.97	Re -0.43		Ir -0.63	Pt -0.37	Au -0.65	

CO_2-COOH COOH-CO CO desorption

Fig. S9. The limiting overpotential (U_L) and corresponding PLS for all TM@Gr_s. The orange, purple, and blue represent the PLSs are CO_2-to-COOH step, COOH-to-CO step, and CO desorption step, respectively.

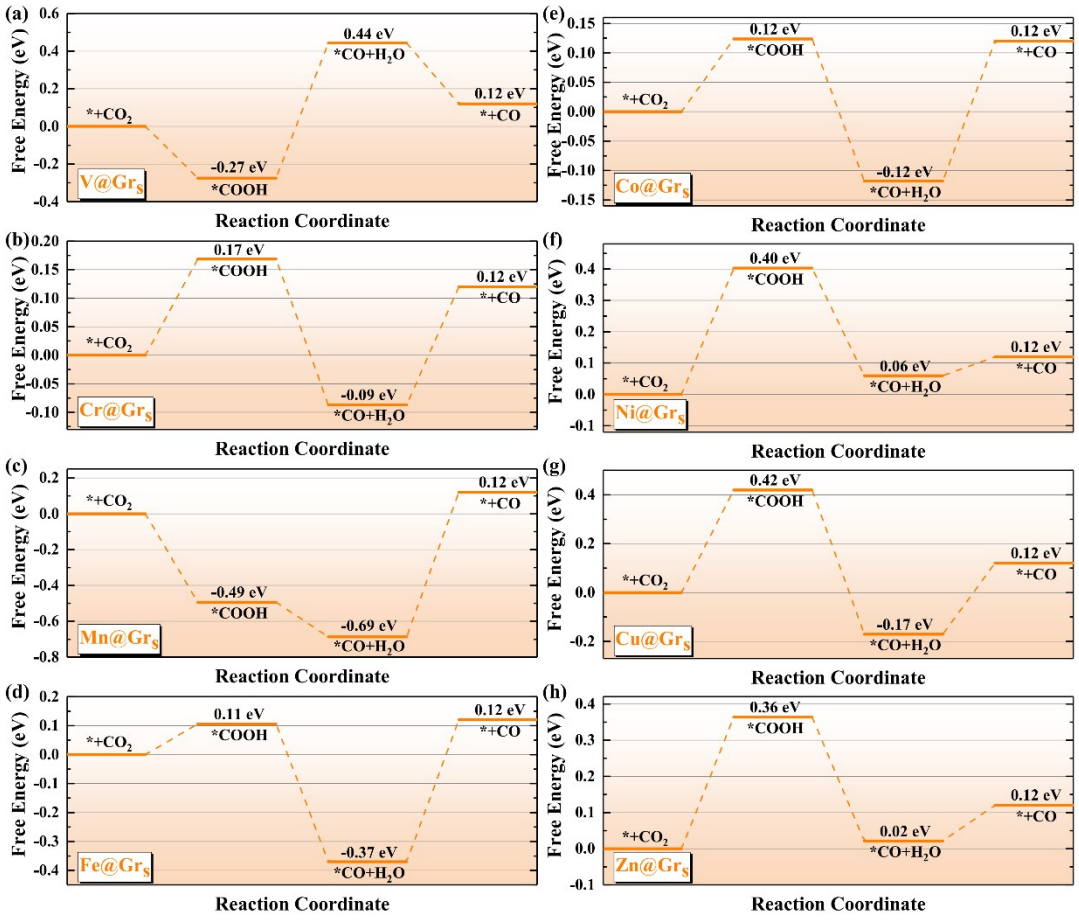

Fig. S10. The Gibbs free energy diagram of CO_2 hydrogenation to CO on the 3d TM@Gr_S SACs.

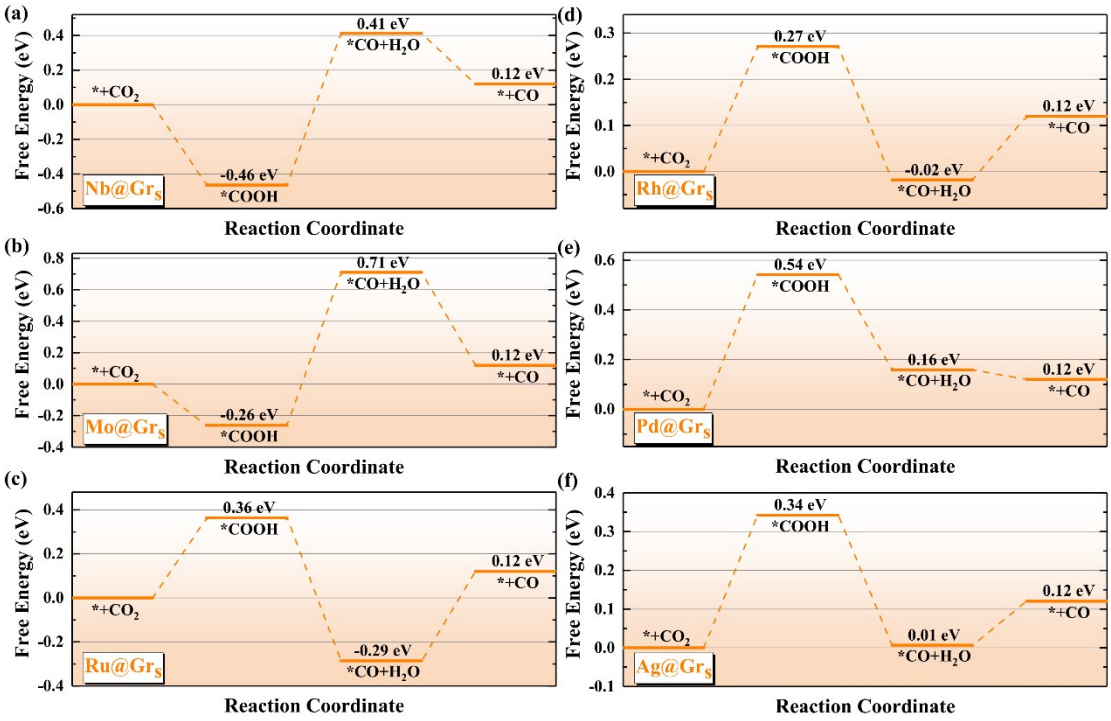

Fig. S11. The Gibbs free energy diagram of CO_2 hydrogenation to CO on the 4d TM@Gr_S SACs.

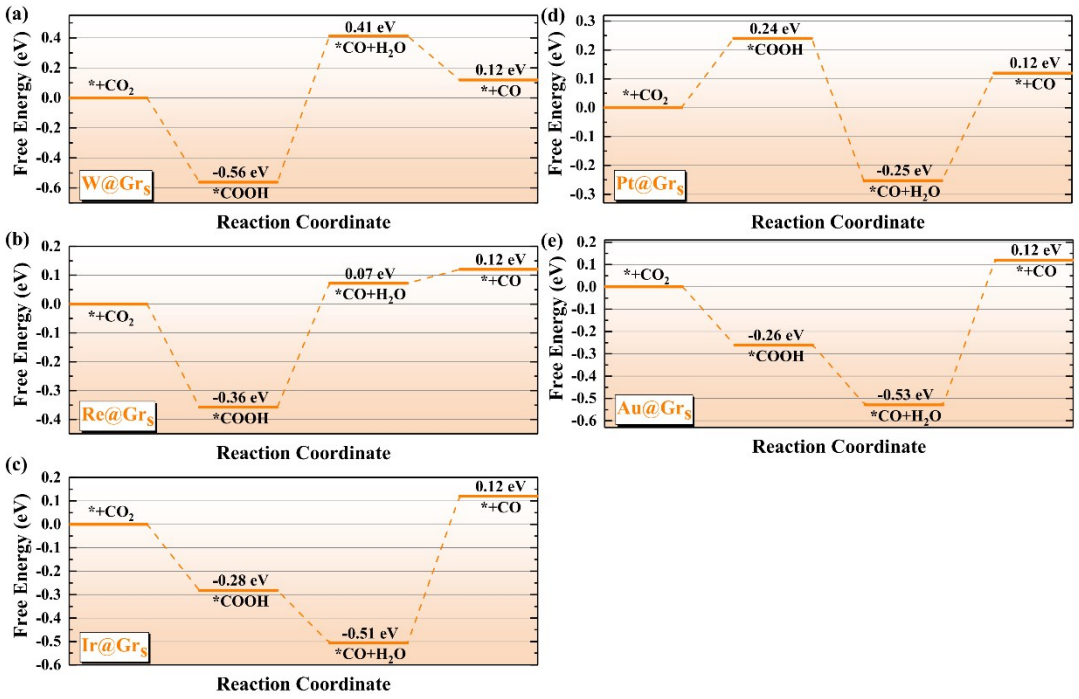

Fig. S12. The Gibbs free energy diagram of CO_2 hydrogenation to CO on the 5d TM@Gr_S SACs.

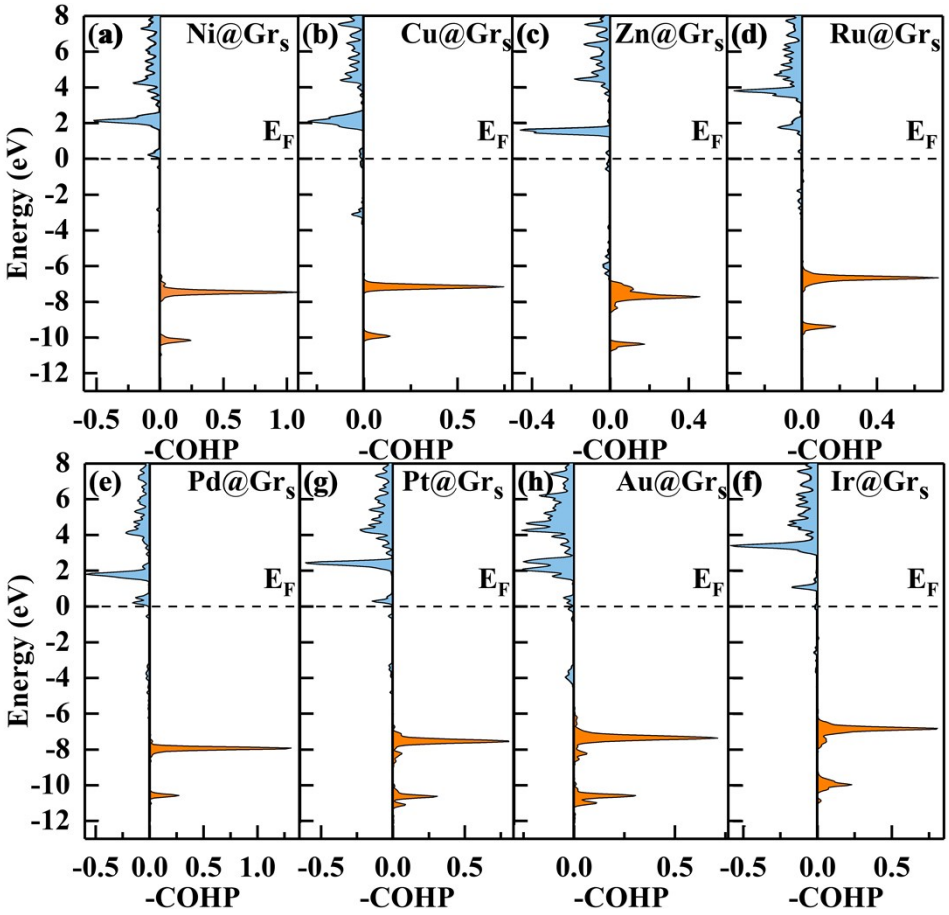

Fig. S13. Projected COHP for CO adsorbed TM@Grs, where TM is (a)Ni, (b) Cu, (c) Zn, (d) Ru, (e) Pd, (f) Ir, (g) Pt and (h) Au, respectively. The bonding (orange) and antibonding (cyan) contributions are displayed on the right and left, respectively.